Liquid−Liquid Phase Behavior of Solutions of 1-Dodecyl-3-methylimidazolium Bis((trifluoromethyl)sulfonyl)amide (C_{12}mimNTf_2) in *n*-Alkyl Alcohols†

Vlad R. Vale,‡ Bernd Rathke,*,‡ Stefan Will,‡ and W. Schröer§

Universität Bremen, Technische Thermodynamik, Badgasteiner Str. 1, 28359 Bremen, Germany, and Universität Bremen, FB2, Institut für Anorganische und Physikalische Chemie, Leobener Str. NWII, 28359 Bremen, Germany

Liquid−liquid phase diagrams of binary mixtures of the ionic liquid 1-dodecyl-3-methylimidazolium bis((trifluoromethyl)sulfonyl)amide (C_{12}mimNTf_2) with *n*-alkyl alcohols (decan-1-ol, undecan-1-ol, dodecan-1-ol, tetradecan-1-ol, hexadecan-1-ol, octadecan-1-ol, and eicosan-1-ol) are reported. Applying the cloud-point method on a set of samples, phase diagrams were obtained at atmospheric pressure in the temperature range of (280 to 423) K. The investigated systems show partial miscibility with an upper critical solution temperature between (288 and 352) K. With increasing chain length of the alcohols, the critical point is shifted toward higher temperatures and slightly higher concentrations, while the shape of the phase diagrams is nearly unaffected. Ising criticality is presumed for the numerical analysis of the phase diagrams. The analysis yields the data of the critical point and the parameters of the width and of the asymmetry which characterize the shape of the phase diagrams. The temperature dependence of the diameter of the phase diagrams, which describes the asymmetry, is not linear as presumed by the rectilinear diameter rule of Cailletet−Mathias but, as requested by scaling theories of critical phenomena, depends also on nonlinear, nonanalytical contributions that are the leading terms when approaching the critical solution point. For the mixture of C_{12}mimNTf_2 + dodecan-1-ol the critical point was determined independently using the equal-volume criterion. Taking into account the nonlinear temperature dependence of the diameter, the data of the critical point estimated from the fit of the phase diagram are in good agreement with those determined by the equal volume criterion.

Introduction

Phase diagrams of liquid−liquid equilibria are important basic data for chemical engineering applications.[1] A reliable description of phase diagrams with a minimum of parameters is useful and requires a sound theoretical basis.[2] By now, it is common knowledge that the critical behaviors of the liquid−gas and the liquid−liquid phase transition of nonionic systems both show the characteristic features of the 3D-Ising model.[2−5] This is remarkable because of the simplicity of the model, which considers particles on a lattice in three dimensions that have two possible states and only accounts for next-neighbor interactions described by a single parameter, the sign of which is positive for neighboring particles in the same state and negative in the other case. This model allows for a phase transition, where the two phases differ by the relative occupation of the two states. When applying the Ising model for analyzing phase diagrams of the liquid−gas or the liquid−liquid phase transition, the relative occupation of the two states in the Ising model is identified with a composition variable, e.g., the density or the mole fraction. The temperature dependence of the difference between compositions in the coexisting phases is universally determined by the power law $|T - T_c|^\beta$ depending on the separation of the transition temperatures T from the critical temperature T_c. The exponent β takes up the universal value $\beta = 0.326$.[2−5] In variance to experiments that state Ising critical behavior, all mean-field theories like the van der Waals theory[6] or the theory of regular solution and their sophisticated generalizations always yield $\beta = 1/2$.[2,6,7]

It has been proven by theory that the Ising model applies if the phase transition is driven by short-range interactions, which means that the interaction decays with r^{-n}, where $n \geq 4.97$.[8] Therefore, it was discussed that in ionic systems—if Coulomb interactions determine the phase transition—the nature of the phase transition may be different because of the long-range nature of the Coulomb interactions that vary with r^{-1}.[9−12] Thus, the phase behavior of ionic systems is of fundamental interest: In variance to the Ising behavior found in nonionic fluids, mean-field criticality was hypothesized for describing the phase transitions of ionic fluids.[9−12] However, experiments on ionic solutions corroborating this hypothesis[13,14] could not be reproduced.[15] According to experiments[15−21] and simulations,[22−24] it is now almost certain that the liquid−gas phase transition of salts and the liquid−liquid phase transition in ionic solutions also show Ising behavior because the correlations become short-ranged[25−27] due to cooperative shielding of the ions as already described by the Debye−Hückel theory. It is quite likely that experimental deficiencies are the reason if anything other than Ising criticality is found.[21] For reviews on the story of criticality in Coulomb systems, see refs 28 and 29.

However, there is a marked difference between the phase diagram of the Ising model and that of real systems. In variance to the Ising model, the phase diagrams of fluids are in general asymmetric. The asymmetry implies that the average composition of the two phases, termed diameter, is not constant but varies with temperature. The asymmetry of the phase diagrams

† Part of the "Sir John S. Rowlinson Festschrift".

* To whom correspondence should be addressed. Tel.: +49 421 218 3334. Fax: +49 421 218 7555. E-mail: rathke@uni-bremen.de.
‡ Technische Thermodynamik.
§ Institut für Anorganische und Physikalische Chemie.

10.1021/je100359x
Published on Web 07/14/2010

was known from the time of the first measurements of phase diagrams and is already included in the van der Waals equation.[2,6] However, the van der Waals equation and all mean-field theories predict that the diameter of the phase diagram varies linearly with the temperature[2,6,7] near the critical point. This behavior, which is termed the rectilinear diameter rule of Cailletet−Mathias,[30] appeared well established for almost a century. It was used as a tool for estimating critical data.[2] However, a careful analysis reveals that the temperature dependence of the diameter is not linear and becomes even nonanalytical when approaching the critical point, which means that a Taylor expansion at the critical point with natural numbers as exponents is not possible. Widom and Rowlinson were the first to point out this behavior from the theoretical analysis of the model fluid of penetrable soft spheres.[31] They predicted that the diameter should have a temperature dependence of $|T - T_c|^{1-\alpha}$, where $\alpha = 0.11$ is the critical exponent determining the divergence of the specific heat when approaching the critical temperature.[2−5] It was observed that another nonanalytical term determined by the exponent 2β was often required for describing the temperature dependence of the diameter.[32,33] This term was regarded as spurious, resulting from a "wrong choice" of the composition variable.[34] However, recent theoretical work leads to the conclusion that the diameter in general is a sum of a linear term and nonanalytical terms[35−38] with the exponents $1 - \alpha$ and 2β, respectively. For different choices of the concentration variables, e.g., mole fraction or volume fraction, the relative importance of those terms varies, which may lead to a small amplitude of the 2β-term or even to apparent cancellation of the nonanalytic terms, so that the linear approximation appears to work well in many cases.[37] The asymmetry of the phase diagrams of ionic systems has been known to be particularly large for a long time,[39] but systematic investigations have not been reported.

Ionic liquids (ILs),[40] which are defined as salts with melting points below 373 K, allow for such investigations. The investigation of ILs is a most active field of research at present because of their high potential for applications, e.g., for extractions.[41−44] Thus, thermodynamic data of ILs and their solutions are of actual interest. Quite a few data (the list is not exhaustive) on phase diagrams of solutions of ILs have been reported.[45−67] Nevertheless, systematic studies are still required for assessing the relations between the phase diagrams and the chemical structures of the components by empirical analysis and theoretical methods. This work is part of an ongoing series of investigations on this field and aims to contribute to this program. Investigations of mixtures with alcohols are informative because variation of the chain length of the alcohols changes the dielectric permittivity ε of the solvent allowing for a systematic study of the influence of the dielectric permittivity on the phase diagrams. In principle, such investigations can cover the range from highly polar to nonpolar solvents,[45,46,54] e.g., from water ($\varepsilon(T = 298.15\ \text{K}) = 78.38$[68])[45−47] to hydrocarbons (typical value $\varepsilon(T = 298.15\ \text{K}) = 1$ to 2[68]).[54−57,65] Phase diagrams of solutions of ILs with the anions BF_4^- or PF_6^- have been reported in some detail.[45−53] Some work on phase behavior of solutions of ILs with halide-anions has been reported.[54−57] ILs with the anion bis((trifluoromethyl)-sulfonyl)amide (NTf_2^-) are of actual interest because this anion is rather hydrophobic, and thus the ILs are solvable in nonpolar solvents. ILs with the NTf_2-anion are more stable against hydrolysis than ILs with the anions BF_4^- or PF_6^-.[69] Work on solutions of ILs with the NTf_2^- anion concerns solutions in aprotic solvents[58−61] and alcohol solutions.[51−53,62−67] We extend

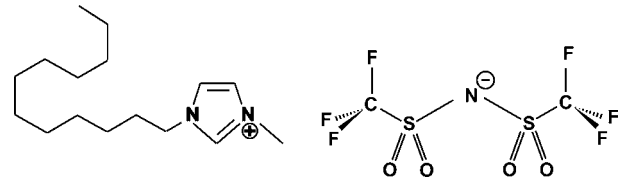

Figure 1. Structure of the ionic liquid 1-dodecyl-3-methylimidazolium bis((trifluoromethyl)sulfonyl)amide, abbreviated as $C_{12}mimNTf_2$.

investigations[51−53,62−66] concerning mixtures of ILs with the NTf_2^- anion with the rather polar *n*-alkyl alcohols of small chain length ($n = 2$ to 6) toward solutions of less polar alcohols with larger chain lengths ($n = 10$ to 20). For the sake of clarity, the dielectric permittivities of the alcohols used were calculated for a fixed temperature of $T = 298.15$ K and are given in the Experimental Section. The investigation of phase diagrams with long-chain alcohols at ambient conditions requires ILs that have cations with longer side chains and thus are more hydrophobic. However, varying the length of the side chain of the methyl-imidazolium cations not only causes a change of the hydrophobicity of the ILs but also causes structural changes. With increasing length of the side chain, the methyl-imidazolium salts $C_x$mim show an increasing tendency for microscopic segregation of the salts into ionic and hydrophobic regions.[70,71] For longer side chains ($x > 10$), liquid-crystalline domains are formed for salts with the anions Cl^-, Br^-, BF_4^-, and PF_6^- but not with the NTf_2^- anion[72] which is definitely nonspherical and has different conformers.[73] We report here seven phase diagrams of mixtures of 1-dodecyl-3-methylimidazolium bis((trifluoromethyl)sulfonyl)amide ($C_{12}mimNTf_2$) with *n*-alkyl alcohols ($n = 10$, 11, 12, 14, 16, 18, and 20) (Figure 1) supplementing our previous report on solutions of C_8mim NTf_2 and C_{10}mim NTf_2.[67] For the investigated mixtures, the liquid−liquid phase transition is in the region of the liquid solid transition of both the salt ($T_m = 289.85$ K)[72] and the alcohols[74] which may cause complications of the phase diagrams of the solutions of $C_{12}mimNTf_2$ when compared with the solutions of ILs with shorter length of the side chain of the imidazolium cation.

The phase diagrams are obtained by the synthetic method, which means that transition temperatures in a set of samples are measured. The transition temperatures, termed cloud-points, are determined by visually observing the onset of the phase separation. The numerical data analysis yield the location of the critical point and the parameters describing the shape of the phase diagrams. In general, it is very difficult to obtain reliable figures for the various terms. This statement holds for the most precise measurements carried out with 10^{-3} K accuracy on a flame-sealed sample of critical composition[15−17] and is even more pronounced when determining the phase diagrams using the cloud-point method because the accuracy of the cloud-point method is limited by uncontrollable traces of impurities of the different samples and by the uncertainty to determine the onset of the phase transition especially because of the appearance of metastable states and kinetic hindrance of phase separation. Nevertheless, it was observed in former work[60] that replacing the linear diameter by a nonlinear term led to a substantial improvement of the data representation obtained by the cloud-point method.

Thus, in the data analysis, Ising criticality is presumed, and a linear and/or a nonanalytical term are taken into account for modeling the diameter. We investigate if by considering a nonanalytic temperature dependence of the diameter an improvement of the fits to the phase diagrams is achieved. For the solution in $C_{12}OH$, we will also compare the estimates for

the critical point obtained by the different approximations used in the fits with those obtained experimentally by the equal volume criterion.

Experimental Section

Materials. The *n*-alkyl alcohols decan-1-ol ($C_{10}H_{22}O$, CAS No. 112-30-1, purity mass fraction $w \geq 0.99$; $\varepsilon(T = 298.15\ K) = 7.66$[68]), undecan-1-ol ($C_{11}H_{24}O$, CAS No. 112-42-5, purity $w \geq 0.98$; $\varepsilon(T = 298.15\ K) = 6.74$[68]), dodecan-1-ol ($C_{12}H_{26}O$, CAS No. 112-53-8, purity $w \geq 0.99$; $\varepsilon(T = 298.15\ K) = 6.53$[68]), tetradecan-1-ol ($C_{14}H_{30}O$, CAS No. 112-72-1, purity $w \geq 0.98$; $\varepsilon(T = 298.15\ K) = 5.19$[68]), hexadecan-1-ol ($C_{16}H_{34}O$, CAS No. 36653-82-4, purity $w \geq 0.95$; $\varepsilon(T = 298.15\ K) = 4.15$[68]), octadecan-1-ol ($C_{18}H_{38}O$, CAS No. 112-92-5, purity $w > 0.99$; $\varepsilon(T = 298.15\ K) = 3.80$[68]), and eicosan-1-ol ($C_{20}H_{42}O$, CAS No. 629-96-9, purity $w \geq 0.96$; $\varepsilon(T = 298.15\ K) = 3.50$[68]) were purchased from Merck (Merck KGaA, Darmstadt, Germany) with a maximum of available purity and were used without further purification. The ionic liquid 1-dodecyl-3-methylimidazolium bis((trifluoromethyl)sulfonyl)amide ($C_{18}H_{31}F_6N_3O_4S_2$, $C_{12}mimNTf_2$, CAS No. 404001-48-5, purity $w > 0.98$; water $w < 10^{-4}$), purchased from IoLiTec (Ionic Liquids Technologies GmbH, Heilbronn, Germany), was degassed and dried before sample preparation. To remove the water and any volatiles, the ionic liquid $C_{12}mimNTf_2$ was filled into a 100 mL round-bottom flask (Schott Duran glass) under an inert argon atmosphere inside a glovebag (AtmosBag, Sigma-Aldrich) and dried under continuous stirring at a temperature of 318 K for about 12 h under a vacuum of $2 \cdot 10^{-5}$ bar. The drying process was frequently monitored by weighing the sample. We checked the mass loss of a sample of typical 40 g of IL after the process of drying and found that the detectable loss of mass was less than 10^{-3} g within a period of 2 h.

Sample Preparation. The phase diagrams were determined using the synthetic method: Mixtures of ionic liquid and alcohol of different composition were prepared in culture tubes (glass type: Schott Duran) with heat-resistant screw caps made of PBT with a sealing made of PTFE-coated silicon under a protective gas atmosphere (argon), thus avoiding contact with air and humidity. In minimum, ten samples with molar fractions between 0.02 and 0.45 were prepared for each binary mixture weighing each component directly into the sample tubes; the typical size of a sample was 2 g. The composition was determined gravimetrically with an accuracy of 10^{-3} g which results in an overall uncertainty of the mole fraction of $\Delta x_{IL} = \pm 10^{-3}$.

Cloud-Point Detection. The transition temperatures defining the liquid−liquid phase diagrams of the IL−alcohol binary mixtures were determined by the cloud-point method. For measurements in the lower-temperature region, $T =$ (290 to 340) K, a transparent water-bath was used. The temperature stability was ± 0.02 K controlled by a thermostat (Haake DC 30, Thermo, Karlsruhe, Germany). In the higher-temperature range, $T =$ (340 to 430) K, measurements were carried out in a silicon oil bath with a temperature stability better than ± 0.05 K (Lauda, Proline RP845/PV15). In either case, the temperature was measured using a Pt-100 sensor connected to a high-precision resistance thermometer (Kelvimat 4323, Burster, Gernsbach, Germany) with an uncertainty of ± 0.05 K.

The cloud-point temperatures were determined visually as the onset of the phase transition. For this purpose, the temperature range and the temperature steps in the considered range were systematically reduced. At first, the prepared samples with known mole fraction were heated to about 5 K above the critical temperature for about 20 min and homogenized using either a Vortex mixer or a magnetic stirrer. The temperature was then decreased in steps of typically (0.5 to 5) K until the two-phase region was reached. The temperature was increased again until the sample reached the one-phase region. These steps were repeated until the temperature interval in which the cloud-point temperature was observed within a time up to 10 min reached 0.1 K near the critical point and (0.1 to 0.3) K near the edges of the phase diagrams. The cloud points and their repeatability were determined by repeating this procedure up to five times starting from the one-phase region at different initial temperatures followed by reducing the temperature in steps of 0.05 K at the top of the phase diagrams and in steps of (0.2 to 1) K at the edges. The cooling rate was also varied between (0.05 and 1) $K \cdot min^{-1}$ because first-order phase transitions, especially at the edges of the phase diagram, may occur under highly supersaturated conditions so that the onset of demixing depends on the speed of penetration into the metastable region. By this procedure, uncertainties are minimized that arise from the subjectivity of the observer, the appearance of metastable states, and kinetic effects. The uncertainties δT of the cloud-point temperatures T_{cloud} given in Table 1 are estimated from the accuracy of the T measurement and the repeatability of observed transition temperatures. The influence of uncontrollable traces of impurities of the substances, which might affect the results in a systematic way, is not taken into account. However, checks on different batches of the substances used in this study showed no significant variations. Together with the statistical error, this results in a slight scatter of the cloud-point temperatures which could be estimated from the standard deviation of the fits from the experimental data.

Determination of the Critical Composition. For the solution in dodecan-1-ol, the critical composition was determined by the equal-volume criterion. According to this criterion, the volume in the coexisting phases at the critical composition should be equal. To determine the corresponding composition, four larger samples of a volume of 5 mL of near critical composition were prepared. The formation of a second phase was detected as described above. The temperature of the observed separation was then kept constant for 2 h, and the levels of the coexisting phases inside a graded sample tube were measured with an uncertaity of 0.05 cm^3. For samples with the mass fractions $w =$ (0.291 ± 0.001, 0.310 ± 0.001, and 0.350 ± 0.001), the volume ratios (lower to upper phase) were determined to $v_l/v_u =$ (0.615 ± 0.079, 1.294 ± 0.039, and 3.000 ± 0.012). The mass fraction $w = 0.304 \pm 0.002$ of a fourth sample of which the equal volume ratio should apply was estimated by interpolation. The volume ratio of this sample was $v_l/v_u = 1.04 \pm 0.038$, so that this sample had almost critical composition. Further interpolation yields $w_c = 0.302 \pm 0.002$ for the critical mass fraction or $x_c = 0.132 \pm 0.001$ for the critical mole fraction.

Results and Discussion

Experimental Results. The data of the phase diagrams are listed in Table 1. We give the mass fractions, the mole fractions, the cloud-point temperatures, and the uncertainties of the measurements for the solutions of $C_{12}mimNTf_2$ in the alcohols decan-1-ol ($C_{10}OH$), undecan-1-ol ($C_{11}OH$), dodecan-1-ol ($C_{12}OH$), tetradecan-1-ol ($C_{14}OH$), hexadecan-1-ol ($C_{16}OH$), octadecan-1-ol ($C_{18}OH$), and eicosan-1-ol ($C_{20}OH$). The phase diagrams are shown in Figures 2a, b, c, and d. Figure 2a shows the complete set of phase diagrams of the mixtures of $C_{12}mimNTf_2$ with the alcohols $C_{10-20}OH$ obtained in this study;

Table 1. Data Set for the Liquid−Liquid Phase Diagrams of C_{12}mimNTf$_2$ + *n*-Alkyl Alcohol (C_nOH) Mixtures: Mass Fractions *w*, Mole Fractions x_{IL}, and Cloud-Point Temperatures T_{cloud} Including Their Uncertainties δT as a Combination of Accuracy of the *T* Measurement and the Repeatability of the Determination of T_{cloud}[a]

w	x_{IL}	T_{cloud}/K	δT/K
	C_{12}mimNTf$_2$ + decan-1-ol		
0.185	0.063	282.65	0.10
0.232	0.083	287.66	0.10
0.306	0.116	287.96	0.10
0.387	0.158	287.05	0.10
0.450	0.196	287.05	0.10
0.473	0.211	287.01	0.10
0.584	0.295	280.85	0.40
	C_{12}mimNTf$_2$ + undecan-1-ol		
0.061	0.021	283.85	0.10
0.076	0.026	288.35	0.05
0.131	0.046	290.12	0.08
0.155	0.056	291.18	0.06
0.229	0.088	292.25	0.07
0.296	0.120	293.00	0.10
0.300	0.122	292.90	0.10
0.359	0.154	293.20	0.10
0.402	0.179	293.28	0.10
0.405	0.181	293.20	0.10
0.474	0.226	292.60	0.10
0.510	0.252	292.94	0.05
0.556	0.289	291.20	0.10
0.606	0.333	288.85	0.05
0.645	0.371	286.35	0.10
	C_{12}mimNTf$_2$ + dodecan-1-ol		
0.051	0.018	296.36	0.08
0.070	0.024	298.97	0.07
0.148	0.053	304.35	0.08
0.197	0.074	305.57	0.05
0.239	0.092	305.79	0.05
0.244	0.095	305.59	0.10
0.291	0.117	305.83	0.05
0.295	0.120	305.94	0.05
0.304	0.124	305.81	0.05
0.310	0.127	305.80	0.05
0.335	0.140	305.81	0.05
0.350	0.149	305.84	0.06
0.367	0.158	305.87	0.05
0.392	0.173	305.67	0.05
>0.433	0.199	305.54	0.05
0.435	0.199	305.54	0.05
0.452	0.211	305.12	0.05
0.484	0.233	304.66	0.05
0.522	0.261	303.67	0.05
0.555	0.288	302.10	0.10
0.572	0.302	301.85	0.10
0.609	0.335	299.81	0.12
0.631	0.356	298.26	0.12
	C_{12}mimNTf$_2$ + tetradecan-1-ol		
0.054	0.023	311.54	0.30
0.077	0.032	316.35	0.50
0.088	0.037	317.85	0.15
0.141	0.062	319.03	0.07
0.192	0.087	320.45	0.05
0.218	0.101	320.74	0.05
0.293	0.143	320.81	0.05
0.299	0.147	320.83	0.05
0.371	0.192	320.60	0.05
0.439	0.240	319.90	0.05
0.501	0.288	318.44	0.05
0.550	0.330	316.44	0.05
0.577	0.355	314.65	0.10
0.610	0.387	313.55	0.10
	C_{12}mimNTf$_2$ + hexadecan-1-ol		
0.042	0.020	322.75	0.10
0.057	0.027	327.74	0.05
0.116	0.056	330.75	0.08
0.163	0.082	332.25	0.10
0.236	0.124	333.14	0.08
0.309	0.169	333.00	0.08
0.384	0.221	332.55	0.08
0.397	0.231	332.33	0.10
0.483	0.298	330.45	0.12
0.586	0.392	325.98	0.10
0.524	0.334	330.12	0.07
0.055	0.029	334.65	0.50
0.102	0.055	340.25	0.50
0.179	0.100	342.35	0.50
0.261	0.152	342.75	0.30
0.328	0.199	342.65	0.20
0.404	0.257	341.85	0.30
0.431	0.278	341.15	0.30
0.511	0.347	338.85	0.30
0.549	0.382	336.85	0.30
0.618	0.452	332.15	0.40
	C_{12}mimNTf$_2$ + octadecan-1-ol		
0.055	0.029	334.65	0.50
0.102	0.055	340.25	0.50
0.179	0.100	342.35	0.50
0.261	0.152	342.75	0.30
0.328	0.199	342.65	0.20
0.404	0.257	341.85	0.30
0.431	0.278	341.15	0.30
0.511	0.347	338.85	0.30
0.549	0.382	336.85	0.30
0.618	0.452	332.15	0.40
	C_{12}mimNTf$_2$ + eicosan-1-ol		
0.057	0.033	343.85	0.90
0.092	0.054	348.65	0.30
0.160	0.096	350.85	0.30
0.241	0.151	351.65	0.20
0.291	0.187	351.55	0.20
0.378	0.255	350.95	0.20
0.423	0.292	350.35	0.20
0.477	0.339	348.45	0.10
0.558	0.415	344.45	0.50
0.600	0.457	341.75	0.60

[a] The uncertainty in the mole fraction is due to the accuracy of the weight measurement and the sample size $\Delta x_{IL} = \pm 10^{-3}$.

Figure 2b those with C_{10}OH, C_{11}OH, and C_{12}OH; Figure 2c those with C_{14}OH and C_{16}OH; and Figure 2d those with C_{18}OH and C_{20}OH.

The curves drawn in the figures are fits based on eqs 6 and 7 which will be introduced and explained in the next section.

All binary mixtures investigated show phase diagrams of a rather asymmetric shape with an upper critical solution temperature (UCST). The binodals are steep at small concentrations of the salt and become flat at higher concentrations. The critical composition, which in binary mixtures agrees with the maximum temperature of the phase diagrams, is located at low concentrations, in the mole fraction range $0.1 < x_{IL} < 0.2$.

The critical temperatures increase with the chain length of the alcohols. This observation is in agreement with the observations on solutions of ILs with shorter side chain of which measurements of mixtures with alcohols of smaller chain length[62−66] have been reported. Comparing mixtures of ILs differing in the length of the side chain of the cation with the same alcohol, the critical temperatures decrease with the cation size. Thus, phase separation at ambient temperatures with C_{12}mimNTf$_2$ was observable only for solutions of C_nOH with $n = 10$ to 20, while, e.g., for C_8mimNTf$_2$ phase diagrams of *n*-alcohols with $n = 8$ to 20 could be investigated.[67] With increasing length of the side chain of the cation, both the hydrophobicity of the ILs and the solubility in weakly polar organic solvents are enhanced, which corresponds to a decrease of the separation temperature. Analogously reducing the dielectric permittivity of the solvent by a larger chain length of the alcohols reduces the stability of the solutions so that the separation temperature is increased. Those trends are well-known and have been found on solutions of ILs with the anions BF_4^- and PF_6^-[45−53] and can be expected from chemical insight. The variation of the other properties of the phase diagrams with the chain length of the alcohols cannot be extracted by inspection from the phase diagrams. The shape of the curves appears very similar for all systems. The maxima are difficult to determine because the tops of the curves are very flat. Therefore, a numerical analysis of the shape of the phase diagrams is required.

Shape Analysis of the Coexistence Curves. To allow for a quantitative assessment, the phase diagrams were analyzed by fits with an expression yielding the parameters characterizing

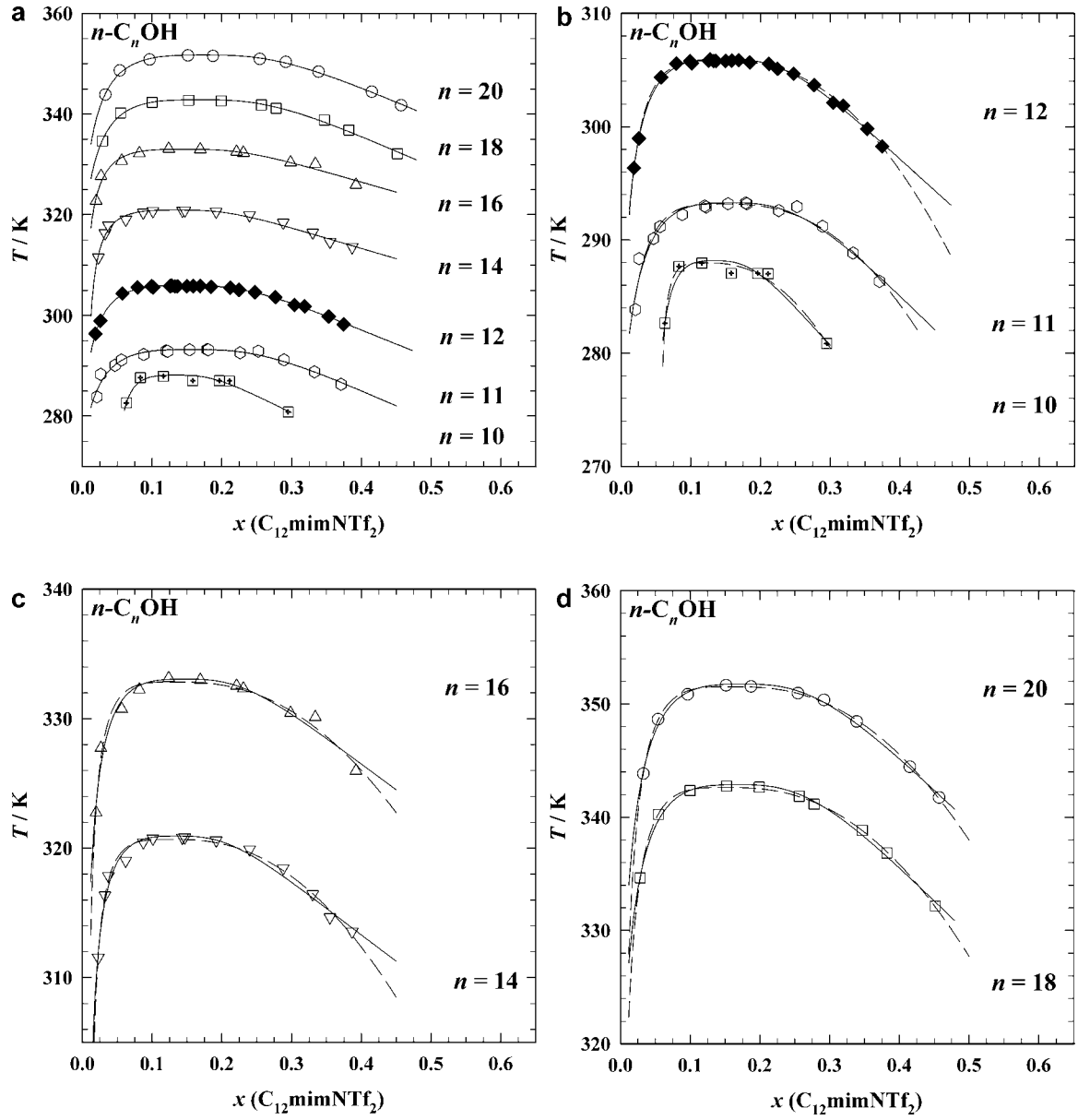

Figure 2. Isobaric phase diagrams at ambient pressure for C_{12}mimNTf$_2$ mixtures with *n*-alkyl alcohols (C_nOH): (a) overview with $n = 10$, 11, 12, 14, 16, 18, and 20; (b) $n = 10$, 11, and 12; (c) $n = 14$ and 16; and (d) $n = 18$ and 20, with the molar fraction x_{IL} as a concentration variable. The uncertainties in T and x are not visible in the resolution of the plot. The lines indicate the curves obtained by fitting the experimental data with eqs 6 (full line) and 7 (dashed line); the parameters are shown in Table 2. The phase diagram for C_{12}mimNTf$_2$ + *n*-dodecanol is plotted with black symbols.

the curves. For the sake of clarity, we recall the main steps yielding the working equations[60] we use for the evaluation of the experimental data. The expressions applied are based on scaling laws used in the field of critical phenomena.[2−5,32,33] Presuming Ising criticality, the temperature dependence of a mole fraction x in the coexisting phases near the critical temperature T_c can be represented by power series in terms of the $T_c - T$ with universal exponents. For mixtures with an upper critical solution point, this expansion reads

$$x_{\pm} = x_m \pm B(T_c - T)^{\beta}(1 + B_1(T_c - T)^{\Delta} + ...) \quad (1)$$

where

$$x_m = x_c + A(T_c - T) + C(T_c - T)^{2\beta} + D(T_c - T)^{1-\alpha} + ... \quad (2)$$

These expansions are nonanalytical because, unlike the Taylor expansion, the exponents are no natural numbers. Furthermore, these expansions are termed singular because the first derivative with respect to the temperature diverges at the critical temperature. The shape of the phase diagram is characterized by the width parameters B and B_1 and the parameters A, C, and D determining the asymmetry of the coexistence curve. The plus in eq 1 refers to the region $x > x_m$ and vice versa, and x_m is the so-called diameter, defined by the average $x_m = (x_+ + x_-)/2$ of the mole fractions x_+ and x_- of the coexisting phases. For the Ising model, the exponents take up the universal values $\beta = 0.326$, $\alpha = 0.11$, and $\Delta = 0.51$, where β is the leading exponent for the phase diagram; α is the exponent of the heat capacity; and Δ is the crossover exponent, describing the crossover from Ising to classical mean-field behavior.[3−5] In mean-field theories, $\beta = 1/2$ and $\alpha = 0$ holds, so that the rectilinear diameter rule of Cailletet−Mathias,[30] which assumes a linear temperature

Table 2. Parameters of the Liquid−Liquid Phase Diagrams of Solutions of the Ionic Liquid C_{12}mimNTf$_2$ in *n*-Alcohols as Obtained by Fitting the Experimental Curves with Equations 5, 6, and 7 Using the Mole Fraction as the Composition Variable[a]

		T_c		B	A	C	σ
solvent	eq	K	x_c	$K^{-1/3}$	K^{-1}	$K^{-2/3}$	K
C_{10}OH	6	288.16 ± 0.49	0.134 ± 0.010	0.0532 ± 0.0050	0.0056 ± 0.0016	-	0.88
	7	287.98 ± 0.30	0.120 ± 0.011	0.0597 ± 0.0022	-	0.0176 ± 0.0045	0.58
C_{11}OH	6	293.27 ± 0.25	0.156 ± 0.008	0.0866 ± 0.0028	0.0062 ± 0.0015	-	0.72
	7	293.17 ± 0.24	0.144 ± 0.009	0.0916 ± 0.0027	-	0.0159 ± 0.0031	0.70
C_{12}OH	6	305.92 ± 0.05	0.147 ± 0.002	0.0821 ± 0.0006	0.0068 ± 0.0003	-	0.18
	7	305.81 ± 0.06	0.136 ± 0.002	0.0887 ± 0.0005	-	0.0168 ± 0.0007	0.17
	5	305.87 ± 0.06	0.140 ± 0.003	0.0856 ± 0.0014	0.0029 ± 0.0013	0.0102 ± 0.0032	0.15
C_{14}OH	6	320.93 ± 0.20	0.135 ± 0.005	0.0797 ± 0.0022	0.0092 ± 0.0009	-	0.52
	7	320.67 ± 0.16	0.125 ± 0.004	0.0914 ± 0.0014	-	0.0231 ± 0.0016	0.41
	5	320.70 ± 0.19	0.125 ± 0.004	0.0899 ± 0.0056	0.0012 ± 0.0042	0.02058 ± 0.0089	0.43
C_{16}OH	6	333.05 ± 0.34	0.146 ± 0.010	0.0873 ± 0.0041	0.0094 ± 0.0019	-	0.79
	7	332.83 ± 0.28	0.131 ± 0.008	0.0978 ± 0.0033	-	0.0245 ± 0.0034	0.67
C_{18}OH	6	342.88 ± 0.18	0.167 ± 0.005	0.0884 ± 0.0018	0.0063 ± 0.0005	-	0.38
	7	342.62 ± 0.05	0.150 ± 0.002	0.0968 ± 0.00039	-	0.0195 ± 0.0006	0.12
	5	342.67 ± 0.06	0.151 ± 0.002	0.0950 ± 0.0012	0.0012 ± 0.0008	0.0163 ± 0.0021	0.12
C_{20}OH	6	351.75 ± 0.15	0.174 ± 0.004	0.0909 ± 0.0017	0.0066 ± 0.0005	-	0.32
	7	351.52 ± 0.08	0.157 ± 0.003	0.0992 ± 0.0006	-	0.0196 ± 0.0010	0.19
	5	351.58 ± 0.11	0.159 ± 0.004	0.0971 ± 0.0025	0.0015 ± 0.0017	0.0157 ± 0.0045	0.20

[a] Critical mole fractions x_c, critical temperatures T_c, widths of the coexistence curve B, and values of the parameters A and C that determine the rectilinear diameter are given, along with their asymptotic standard errors provided by the fitting routine and the standard deviation (σ) of the fits from the experimental data.

dependence of the diameter, applies in mean-field theory.[7] By definition, there is no crossover exponent Δ in mean-field models. While the exponents are universal, the amplitudes are specific for the system but must satisfy certain sum rules. In view of the small temperature range investigated due to the crystallization of the investigated systems and the limited accuracy of the measurements—resolution in the $\Delta T = 10^{-3}$ K range was not in the scope of the present investigation—the correction to scaling with the coefficient B_1, given in eq 1, may be neglected for the analysis[36−38] of the data in this paper. When analyzing data in a wider temperature region (outside the temperature range considered in this investigation), a crossover theory[75] should be applied. However, at large distance from the critical point, other specific contributions must be considered also besides the universal crossover scenario.

The nonanalytic temperature dependence of the diameter had not been noticed for a very long time. Now, the nonlinearity of the diameter is accepted, although its temperature dependence is still under discussion.[35−38] On the basis of the work of Widom and Rowlinson,[31] it was accepted that a term with the exponent $1 - \alpha$ is the leading term near the critical point,[32,33] while the 2β-term was regarded as spurious, resulting from a nonappropriate choice of the concentration variable.[34] Now, the recent developed theory of "complete scaling" requires the 2β-term as the leading part, which is present in general.[35−38] Thus, the search for a "correct" variable that removes the 2β-term is now recognized to be obsolet. However, it is almost impossible to determine uniquely the various coefficients of eq 2 by a numerical analysis of experimental data. This is the case even for data[15−18] of very high precision obtained by investigations on flame-sealed samples of critical composition with temperature stability better than 10^{-3} K. In particular, the temperature dependencies of the linear and of the $1 - \alpha$ term are so similar that a unique determination of both coefficients A and D in a fitting procedure is hardly possible. Therefore, the linear and the $1 - \alpha$ term may be treated as one term if no additional information is available. We presume a linear temperature dependence for this term and approximate the critical exponent β by $\beta = 1/3$, a value which is near the Ising value of $\beta = 0.326$[2,3,5] but more convenient for the numerical analysis than the Ising value. This approximation of β was also used by Guggenheim.[76] The simplified scaling laws applied in the analysis here are

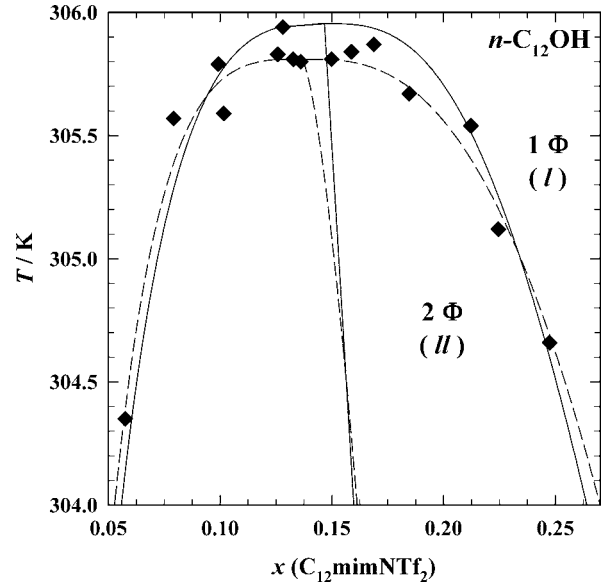

Figure 3. Near critical region and the diameters obtained for the corresponding fits of the isobaric phase diagram at ambient pressure of C_{12}mimNTf$_2$ mixtures with *n*-dodecan-1-ol (C_{12}OH). The uncertainties in T and x are not visible in the resolution of the plot. The lines are calculated with the parameters shown in Table 2, which were obtained by fitting the data with eqs 6 (full line) and 7 (dashed line).

$$x_{\pm} - x_m = \pm B \cdot (T_c - T)^{1/3} \quad (3)$$

where

$$x_m = x_c + A \cdot (T_c - T) + C \cdot (T_c - T)^{2/3} \quad (4)$$

Thus, Ising criticality and the asymmetry of the phase diagrams are taken into account in an approximate manner. In many cases,

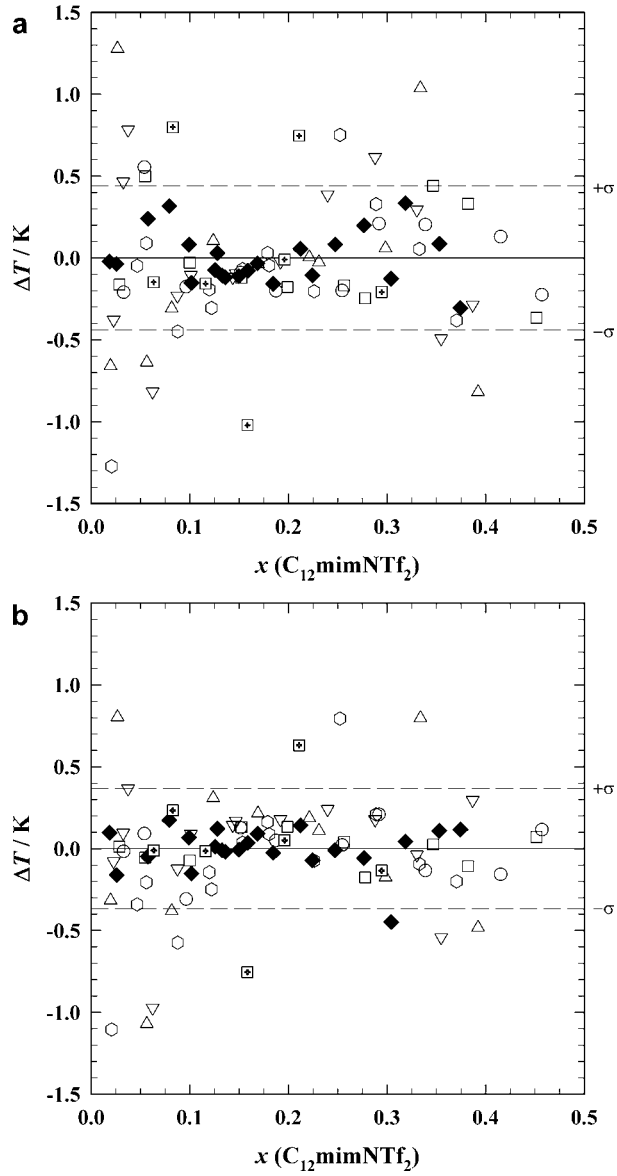

Figure 4. Deviation ΔT of the fitting results for the investigated systems using (a) eq 6 and (b) eq 7; $\Delta T = T_{fit} - T_{exp}$. The overall mean-square deviations σ are marked, and the symbols are the same as that used in Figure 2.

the slope of the diameter is not very large, and an expansion of $|X - X_m|^3$ in first order of A and C may suffice. Solving for T and expressing $T_c - T$ in X_m by the asymptotic power law, the expression for T as a function of X is obtained, which is the basis of the fitting procedure

$$T = T_c - \frac{|x - x_c|^3}{B^3 \pm 3A \cdot |x - x_c|^2 \pm 3CB|x - x_c|} \qquad (5)$$

The positive and negative sign correspond to the range $x < x_c$ and $x > x_c$, respectively. Note that eq 5 takes the nonclassical nature of the phase diagrams into account, while straightforward fits by analytic power series imply classical exponents, which are fundamentally wrong and often lead to erroneous descriptions, e.g., by showing spurious maxima.

It turned out that for most phase diagrams reported in this paper the data do not suffice to allow for a fit by eq 5 yielding all parameters. Only for the mixture of $C_{12}OH$, eq 5 led to a reasonable fit because for this system more data points have been determined than for the other mixtures. Only for this system, it was possible to determine all coefficients of eq 5 with reasonable accuracy by fitting the data. The results are given in Table 2.

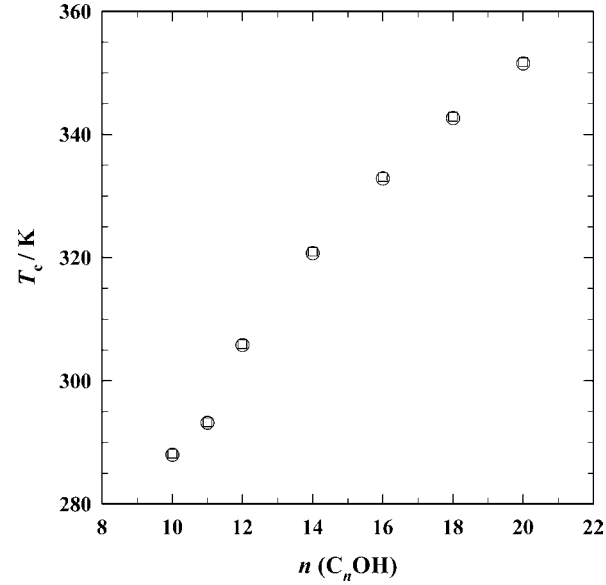

Figure 5. Critical temperatures of the phase diagrams for $C_{12}mimNTf_2$ + n-alkyl alcohol mixtures as obtained by fitting with eq 6 (□) and eq 7 (○). The uncertainties in T_c and differences between the results of the two methods are not visible in the resolution of the plot.

The coefficient A determining the linear term comes out almost a quarter of C, which determines the 2β term. Thus the 2β term is for this system the most important term determining the asymmetry of the phase diagrams. The asymptotic standard errors (ASE) obtained from the Levenberg−Marquardt fit are about 2/5 of the A-value and 1/4 of C. For the other systems, the number of data points is not sufficient to get reliable fits for the parameters in eq 5. In some cases, no stable fit could be obtained. In other cases of which we give the results in Table 2, the ASE figures of the A value typically come out as large as the A-value and about 1/3 of the value of C.

Because eq 5 yielded reliable fit results only for the solution of $C_{12}OH$, we used the simplified versions of eq 5 either presuming—as in a former work—in eq 4 a linear temperature dependence of the diameter determined by the coefficient A

$$T = T_c - \frac{|X - X_c|^3}{B^3 \pm 3A \cdot |X - X_c|^2} \qquad (6)$$

or else taking the 2β term with the coefficient C as the only term determining the asymmetry of the phase diagram.

$$T = T_c - \frac{|X - X_c|^3}{B^3 \pm 3CB|X - X_c|} \qquad (7)$$

The results of those fits are also given in Table 2 together with the ASE for all quantities and standard deviations (σ) of the fits from the data. At first, we concentrate on the mixtures with $C_{12}OH$ of which most data points have been measured. Figure 2b shows the phase diagram of the mixture with $C_{12}OH$ with the fits by eqs 6 and 7. At first glance, the fits with eqs 6 and

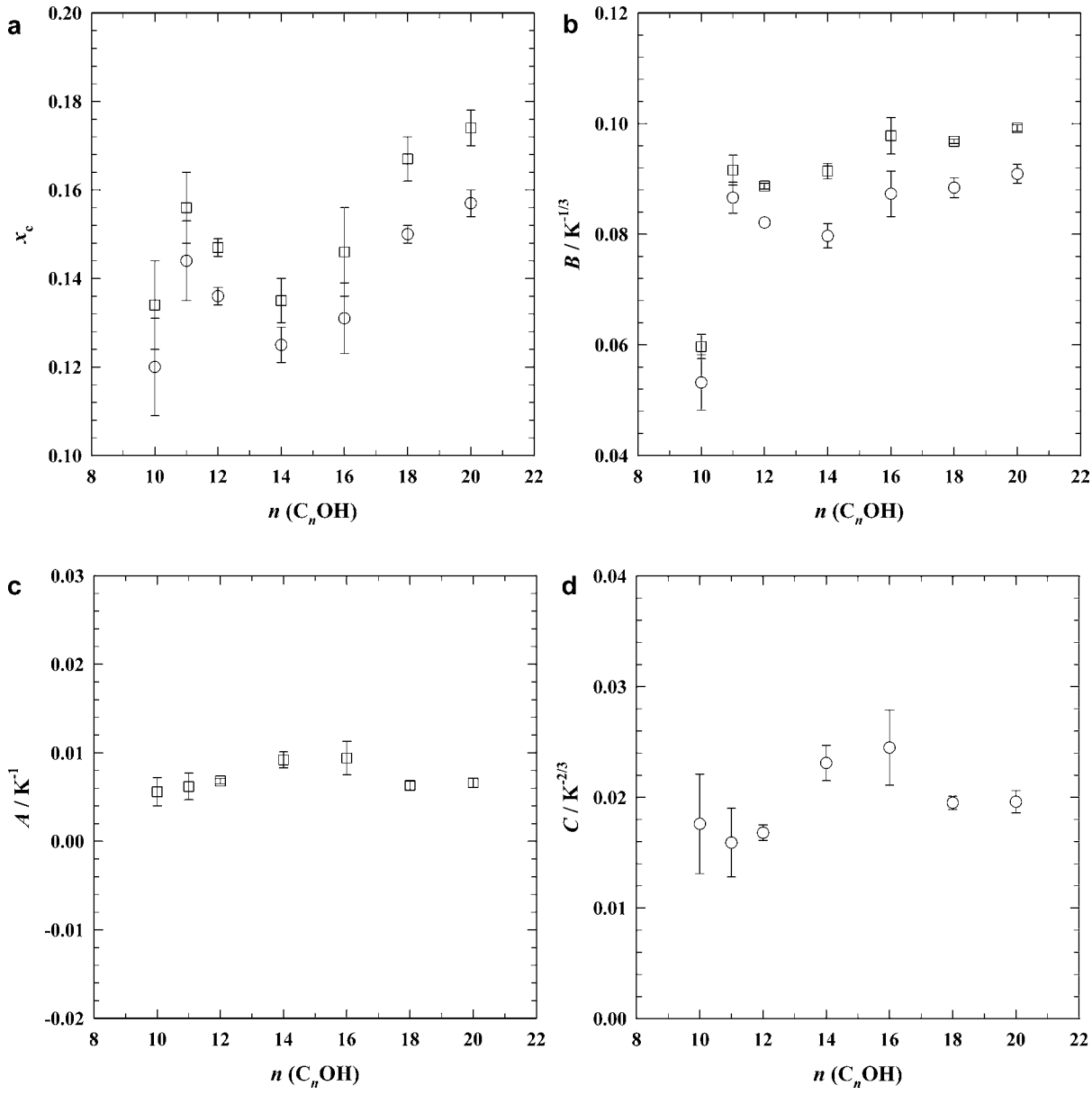

Figure 6. Representation of the characteristics of the phase diagrams for C_{12}mimNTf$_2$ and *n*-alkyl alcohol mixtures as a result of fitting with eqs 6 (□) and 7 (○) as a function of the chain length *n* of the alcohols C$_n$OH. (a) The critical molar fraction x_c, (b) the width of the coexisting region *B*, (c) the parameter *A*, and (d) the parameter *C* which determine the diameter in eqs 6 and 7, respectively.

7 appear to be equally good. Larger deviations are expected only at temperatures outside the investigated region. However, Figure 3, which concentrates on the data within a range of 2 K near the critical temperature, shows that the top of the phase diagram is better described by the fit with eq 7 than by that with eq 6. The fit with eq 5 is very similar to that with eq 7 but is not shown in Figure 3.

The mean-square deviation $\sigma = 0.17$ K obtained with the fit using eq 7 for the phase diagram of the C_{12}OH mixtures is smaller than $\sigma = 0.18$ K obtained by the fit with eq 6. The fit with eq 5 yields the smaller value of $\sigma = 0.15$ K for the mean-square deviation. The residues of the fits of the phase diagrams of the solution of C_{12}OH (black dots) with eqs 6 and 7 shown in Figures 4a and 4b, respectively, illustrate the better performance of the fits with eq 7. This statement is true for all other systems. The mean-square deviations of the fits of the different systems, shown in Table 2, are systematically smaller for the fits with eq 7. The overall standard deviation for the fits with eq 6 of all systems shown in Figure 4a is $\sigma = 0.44$ K, which is above the corresponding value of $\sigma = 0.37$ K for the fits based on eq 7.

We now turn to discuss the results for the critical temperature and the critical mole fraction of the C_{12}OH solution. For the C_{12}OH solution, the resulting estimates of the critical temperature are T_c = (305.87 ± 0.06, 305.92 ± 0.05, and 305.81 ± 0.06) K for the fits with eqs 5, 6, and 7, respectively, which is within the accuracy of the measurements.

The results for the critical composition as obtained by the different fit methods are rather different: the fit assuming the validity of the rectilinear diameter rule yields a figure for the critical composition, which is about 0.01 higher than that obtained by the fit taking only the 2β term into account. This is visualized in Figure 3, which shows also the diameter as estimated from the results of the fits with eqs 6 and 7. The diameter near the critical region is given by $T_m = T_c - (x_m - x_c)/A$ or $T_m = T_c - ((x_m - x_c)/C)^{3/2}$ for the fits with eqs 6 and

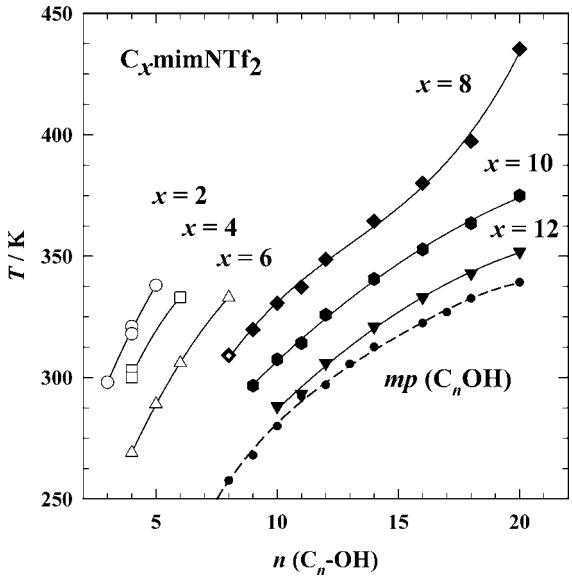

Figure 7. Dependence of the UCST on the chain length of C_nOH for different $C_x$mimNTf$_2$ ($x = 12$, this work; black triangles) and data from the literature (open symbols)[52,53,65,66] and of our previous own work (filled symbols).[67] The melting temperatures of the alcohols (labeled as mp(C_nOH))[74] are also shown to illustrate the principle chain-length dependency of the UCSTs of the investigated systems. Lines in the picture are given to illustrate trends and to guide the eye.

7, respectively. The bend of the nonlinear diameter in eq 7 leads to a smaller figure for the estimate of critical mole fraction than the fit with eq 6.

Comparison with the value of the critical composition $x_c = 0.132 \pm 0.002$ determined experimentally by the equal volume criterion for the C_{12}OH system shows that the estimates ($x_c = 0.136 \pm 0.002$) obtained by the fits taking the 2β term into account agree much better with the experimental figure than the value of $x_c = 0.147 \pm 0.002$ obtained by the fit with eq 6. Thus, it may be concluded that the phase diagram is better described by eq 7 that describes the diameter by the 2β term than by eq 6 based on the rectilinear diameter rule, although the number of parameters is unchanged.

We now turn to discuss the results for the parameters obtained by the fits. The results for the fits of the various systems are given in Table 2. The few data for the solutions of C_{10}OH, which are obtained near the lower temperature limit accessible with the equipment used for this investigation, do not allow for a reliable fit but are given for the sake of completeness. We discuss how the parameters T_c, x_c, B, A, and C vary with the chain length of the *n*-alkyl alcohol. With a first glance at Table 2, it seems that with the exception of the critical temperature T_c all other variables, namely, the critical mole fraction x_c, the parameter of the width B, and the parameters determining the diameter A and C, do not vary much with the chain length of the alcohols. Nevertheless, Figures 5 and 6a, b, c, and d show some regular variation.

Figure 5 shows the critical temperatures T_c of the various systems. The critical temperatures increase with the chain length of the alcohols. The slope of this trend is reduced with the chain length of the alcohols. This is different from the behavior of ILs with shorter side chain of the imidazolium cation, where an increase of the slope was found.[67] A similar behavior was observed for alcohol solutions of $C_n$mimBF$_4$ and $C_n$mimPF$_6$.[46]

Figures 6a to d show the critical mole fraction x_c of the parameter of the width B and the parameters A and C determining the diameter as a function of the chain length of the alcohols.

The critical compositions, shown in Figure 6a, are in a region $0.12 < x_c < 0.18$. The fits based on eq 6 always yield numbers which are about 0.01 larger than those obtained from eqs 5 and 7. Comparing the data of the different alcohol solutions, it seems that the critical composition has a local minimum around $n = 14$, while the analysis of the phase diagrams of the solutions of C_8mimNTf$_2$ and C_{10}mimNTf$_2$ in *n*-alkyl alcohols, which we have reported before,[67] yielded a small monotonous increase with the chain length of the alcohols without noticeable structure. Similar behavior is found for the other parameters.

The values of the parameters B of the width, shown in Figure 6b, are between (0.08 and 0.1) $K^{-1/3}$. The figures vary little for the solutions in the different alcohols. Here, the values resulting from the fits with eq 7 are systematically below those from the fits with eq 6 and appear to indicate a minimum near $n = 14$.

The parameters A and C describing the diameter, shown in Figures 6c and 6d, also do not vary much with the chain length of the alcohols. Here we notice independently of the fit formula applied a maximum in the region where x_c and B show indications of a minimum.

General Discussion. With the exception of the critical temperature, all parameters describing the phase diagrams vary little for the different alcohol solutions as one might expect by comparing the curves shown in Figures 2a,b,c. The critical mole fraction and the width appear to pass a shallow local minimum in the region of the alcohol chain length around $n = 14$, while the asymmetry appears to pass a maximum in this area.

To put our results in the context of other work where phase diagrams with shorter side chains of $C_x$mimNTf$_2$ were investigated, we show in Figure 7 the critical temperatures determined for our systems together with those from the literature[52,53,65,66] and of the former report.[67]

As the critical temperatures for mixtures with C_{12}mimNTf$_2$ approach the region of the melting temperatures of the pure alcohols, the latter are also included.[74] Remarkably, a similar shape for the curves describing the dependence of the critical temperatures on the length of the alcohols and of the melting temperatures of the alcohols is observed. Figure 7 shows the systematic increase of the UCST with increasing chain length of the alcohols. The increase of the critical temperatures of the alcohol mixtures with C_{12}mimNTf$_2$ is, however, reduced with increasing chain length of the alcohols, which is different from the behavior found for $C_n$mimNTf$_2$ solutions with $n < 10$ where the increase of the critical temperatures is enhanced.

A further elucidation of the critical points and of the shape of the phase diagrams by searching for correlations with other properties such as the dielectric permittivities, the densities, or molecular structures is outside the scope of this work and will be given elsewhere.

Concerning the data analysis, it is remarkable that by taking into account the Ising nature and the asymmetry of the phase diagram a good data description was achieved with a minimum number of free parameters. The description of the temperature dependence of the diameter by the 2β term turned out to be superior to that presuming the validity of the rectilinear diameter rule. Taking into account the theoretically based critical exponents of the phase diagram is advantageous even for data obtained by the cloud-point method which are limited in their precision.

Acknowledgment

We thank A. Heintz, R. Ludwig, and S. Verevkin for discussions and shared insight.

Literature Cited

(1) Prausnitz, J. M.; Lichtenthaler, R. N.; de Azevedo, E. G. *Molecular Thermodynamics of Fluid Phase Equilibria*, 2nd ed.; Prentice-Hall Inc.: Englewood Cliffs, 1986.

(2) Rowlinson, J. S.; Swinton, F. L. *Liquids and Liquid Mixtures*, 3rd ed.; Butterworths: London, 1982.

(3) Domb, C. *The Critical Point*; Taylor and Francis: London, 1996.

(4) Anisimov, M. A. *Critical Phenomena in Liquids and Liquid Crystals*; Gordon and Breach: Philadelphia, 1991.

(5) Ivanov, D. Y. *Critical Behavior of Non-Ideal Systems*; Wiley-VCH: Weinheim, 2008.

(6) *J. D. van der Waals on the continuity of the gaseous and liquid states*; Rowlinson, J. S., Ed.; Studies in Statistical mechanics, North-Holland: Amsterdam, 1988; Vol. XIV.

(7) Sengers, J. V.; Levelt Sengers, J. M. H. Critical Phenomena in Classical Fluids. In *Progress in Liquid Physics*; Croxton, C. A., Ed.; Wiley: Chichester, 1978; pp 103−174.

(8) Kayser, R. F.; Raveche, H. J. Asymptotic density correlations and Corrections to Scaling for fluids with non-finite -range Interactions. *Phys. Rev. A* **1984**, *29*, 1013–1015.

(9) Pitzer, K. S. Critical Phenomena in Ionic Fluids. *Acc. Chem. Res.* **1990**, *23*, 333–338.

(10) Fisher, M. E. The Story of Coulombic Criticality. *J. Stat. Phys.* **1994**, *75*, 1–36.

(11) Stell, G. Criticality and Phase-Transitions in Ionic Fluids. *J. Stat. Phys.* **1995**, *78*, 197–238.

(12) Weingärtner, H.; Schröer, W. Criticality of Ionic Fluids. *Adv. Chem. Phys.* **2001**, *116*, 1–66.

(13) Singh, R. R.; Pitzer, K. S. Near-Critical Coexistence Curve and Critical Exponent of an Ionic Fluid. *J. Chem. Phys.* **1990**, *92*, 6775–6778.

(14) Zhang, K. C.; Briggs, M. E.; Gammon, R. W.; Levelt Sengers, J. M. H. The susceptibility critical exponent for a nonaqueous ionic binary mixture near a consolute point. *J. Chem. Phys.* **1992**, *97*, 8692–8697.

(15) Wiegand, S.; Briggs, M. E.; Levelt Sengers, J. M. H.; Kleemeier, M.; Schröer, W. Turbidity, light scattering, and coexistence curve data for the ionic binary mixture triethyl n-hexyl ammonium triethyl n-hexyl borate in diphenyl ether. *J. Chem. Phys.* **1998**, *109*, 9038–9051.

(16) Kleemeier, M.; Wiegand, S.; Schröer, W.; Weingärtner, H. The liquid-liquid phase transition in ionic solution: Coexistence curves of tetra-n-butylammonium picrate in alkylalcohols. *J. Chem. Phys.* **1999**, *110*, 3085–3099.

(17) Oleinikova, A.; Bonetti, M. Coexistence curve of the ionic binary mixture tetra-n-butylammonium picrate in 1-dodecanol. *Chem. Phys. Lett.* **1999**, *299*, 417–422.

(18) Wagner, M.; Stanga, O.; Schröer, W. The liquid-liquid coexistence of binary mixtures of the room temperature ionic liquid 1-methyl-3-hexylimmidazolium tetrafluoroborate with alcohols. *Phys. Chem. Chem. Phys.* **2004**, *6*, 4421–4431.

(19) Schröer, W.; Wiegand, S.; Weingärtner, H. The effect of short-range hydrogen-bonded interactions on the nature of the critical point of ionic fluids. Part II: Static and dynamic light scattering on Solutions of Ethylammonium Nitrate in n-Octanol. *Ber. Bunsen. Ges. Phys. Chem.* **1993**, *97*, 975–982.

(20) Barthel, J.; Carl, E.; Gores, H. J. Coulombic liquid-liquid phase separation of dilithium hexafluoropropane-1,3-bis[sulfonylbis(trifluoromethylsulfonyl)methanide] solutions in diethylcarbonate. *Electrochem. Solid State Lett.* **1999**, *2*, 218–221.

(21) Schröer, W.; Wagner, M.; Stanga, O. Apparent mean-field criticality of liquid-liquid phase transitions in ionic solutions. *J. Mol. Liq.* **2006**, *127*, 2–9.

(22) Caillol, J. M.; Levesque, D.; Weiss, J. J. Critical behavior of the restricted primitive model revisited. *J. Chem. Phys.* **2002**, *116*, 10794–10800.

(23) Orkoulas, G.; Panagiotopoulos, A. Z. Phase behavior of the restricted primitive model and square-well fluids from Monte Carlo simulations in the grand canonical ensemble. *J. Chem. Phys.* **1999**, *110*, 1581–1590.

(24) Yan, Q. L.; de Pablo, J. J. Hyper-parallel tempering Monte Carlo: Application to the Lennard-Jones fluid and the restricted primitive model. *J. Chem. Phys.* **1999**, *111*, 9509–9515.

(25) Leote de Carvalho, R. J. F.; Evans, R. Criticality of ionic fields-the Ginzburg criterion for the restricted primitive model. *J. Phys.: Condens. Matter* **1995**, *7*, L 575−5783.

(26) Lee, B. P.; Fisher, M. E. Ginzburg criterion for Coulombic criticality. *Phys. Rev. Lett.* **1996**, *77*, 3561–3564.

(27) Schröer, W.; Weiss, V. C. Ginzburg criterion for the crossover behavior of model fluids. *J. Chem. Phys.* **1998**, *109*, 8504–8513.

(28) Weingärtner, H.; Schröer, W. Criticality of Ionic Fluids. *Adv. Chem. Phys.* **2001**, *116*, 1–66.

(29) Levelt Sengers, J. M. H.; Harvey, A. H.; Wiegand, S. *Equations of State for Fluids and Fluide Mixtures*; Sengers, J. V., Kayser, R. F., Peters, C. J., White, H. J., Eds.; Elsevier: Amsterdam, 2000; p 805.

(30) See ref 2, pp 72−73.

(31) Widom, B.; Rowlinson, J. S. New model for study of liquid-vapor phase transitions. *J. Chem. Phys.* **1970**, *52*, 1670–1684.

(32) Ley-Koo, M.; Green, M. S. Consequences of the renormalization-group for the thermodynamics of fluids near the critical point. *Phys. Rev. A* **1981**, *23*, 2650–2659.

(33) Greer, S. C.; Das, B. K.; Kumar, A.; Gopal, E. S. R. Critical behavior of the diameters of liquid-liquid coexistence curves. *J. Chem. Phys.* **1983**, *79*, 4545–4552.

(34) Japas, M. L.; Levelt Sengers, J. M. H. Critical behavior of a conducting solution near its consolute point. *J. Phys. Chem.* **1990**, *94*, 5361–5368.

(35) Kim, Y. C.; Fisher, M. E.; Orkoulas, G. asymmetric fluid criticality I. Scaling with pressure mixing. *Phys. Rev. E* **2003**, *67*, 061506.

(36) Cerdeiriña, C. A.; Anisimov, M. A.; Sengers, J. V. *Chem. Phys. Lett.* **2006**, *424*, 414–419.

(37) Wang, J.; Anisimov, M. A. Nature of vapor-liquid asymmetry in fluid criticality. *Phys. Rev. E* **2007**, *75*, 051107.

(38) Wang, J.; Cenderina, C. A.; Anisimov, M. A.; Sengers, J. V. Principle of isomorphism and complete scaling for binary-fluid criticality. *Phys. Rev E.* **2008**, *77*, 031127.

(39) Kirshenbaum, A. D.; Cahill, J. A.; McGonigal, P. J.; Grosse, A. V. The density of liquid NaCl and KCl and an estimate of their critical constants together with those of other alkali halides. *J. Inorg. Nucl.Chem.* **1962**, *24*, 1287–1296.

(40) *Ionic Liquids in Synthesis*, 2nd ed.; Wasserscheid, P., Welton, T., Eds.; Wiley-VCH: Weinheim, Germany, 2008.

(41) Zhao, H. Innovative Applications of Ionic Liquids as "Green" Engineering Liquids. *Chem. Eng. Commun.* **2006**, *193*, 1660–1677.

(42) Plechkova, N. V.; Seddon, K. R. Applications of ionic liquids in the chemical industry. *Chem. Soc. Rev.* **2008**, *37*, 123–150.

(43) *Ionic Liquids: Industrial Applications for Green Chemistry*; Rogers, R. D., Seddon, K. R., Eds.; ACS Symposium Series 818; American Chemical Society: Washington, DC, 2002.

(44) *Ionic Liquids as Green Solvents-Progress and Prospects*; Rogers, R. D., Seddon, K. R., Eds.; Ionic ACS Symposium Series 856; American Chemical Society: Washington, DC, 2003.

(45) Anthony, J. L.; Maginn, E. J.; Brennecke, J. F. Solution Thermodynamics of Imidazolium-Based Ionic Liquids and Water. *J. Phys. Chem. B* **2001**, *105*, 10942–10949.

(46) Wagner, M.; Stanga, O.; Schröer, W. Corresponding states analysis of the critical points in binary solutions of room temperature ionic liquids. *Phys. Chem. Chem. Phys.* **2003**, *5*, 3943–3950.

(47) Cerdeirina, C. A.; Troncoso, I.; Ramos, C. P.; Romani, L.; Najdanovic-Visak, V.; Guedes, H. J. R.; Esperanca, J. M. S. S.; Visak, Z. P.; da Ponte, M. N.; Rebelo, L. P. N. Criticality of the [C(4)mim] [BF4] plus water system: in Ionic liquids: Fundamentals, Progress, Challenges, and Properties and Structure. *ACS Symp. Ser.* **2005**, *901*, 175–186.

(48) Wu, C. T.; Marsh, K. N.; Deev, A. V.; Boxall, J. A. Liquid-liquid equilibria of room-temperature ionic liquids and butan-1-ol. *J. Chem. Eng. Data* **2003**, *48*, 486–491.

(49) Marsh, K. N.; Deev, A.; Wu, C. T.; Tran, E.; Klamt, A. K. Room temperature ionic liquids as replacements for conventional solvents - A review. *Korean J. Chem. Eng.* **2002**, *19*, 357–362.

(50) Sahandzhieva, K.; Tuma, D.; Breyer, S.; Kamps, A.; Maurer, G. Liquid-liquid equilibrium in mixtures of the ionic liquid 1-n-butyl-3-methylimidazolium hexafluorophosphate and an alkanol. *J. Chem. Eng. Data* **2006**, *51*, 1516–1525.

(51) Crosthwaite, J. M.; Muldoon, M. J.; Aki, S. V. N. K.; Maginn, E. J.; Brennecke, J. F. Liquid Phase Behavior of Ionic Liquids with Alcohols: Experimental Studies and Modeling. *J. Phys. Chem. B* **2006**, *110*, 9354–9361.

(52) Crosthwaite, J. M.; Aki, S. N. V. K.; Maginn, E. J.; Brennecke, J. F. Liquid phase behavior of imidazolium-based ionic liquids with alcohols. *J. Phys. Chem. B* **2004**, *108*, 5113–5119.

(53) Crosthwaite, J. M.; Aki, S. N; V, K.; Maginn, E. J.; Brennecke, J. F. Liquid phase behavior of imidazolium-based ionic liquids with alcohols: effect of hydrogen bonding and non-polar interactions. *Fluid Phase Equilib.* **2005**, *228*−*229*, 303–309.

(54) Saracsan, D.; Rybarsch, C.; Schröer, W. Phase separation in solutions of room temperature ionic liquids in hydrocarbons. *Z. Phys. Chem.* **2006**, *220*, 1417–1437.

(55) Domanska, U.; Casas, L. M. Solubility of phosphonium ionic liquid in alcohols, benzene, and alkylbenzenes. *J. Phys. Chem. B* **2007**, *111*, 4109–4115.

(56) Domanska, U.; Paduszynski, K. Phase equilibria study in binary systems (tetra-n-butylphosphonium tosylate ionic liquid+1-alcohol, or benzene, or n-alkylbenzene). *J. Phys. Chem. B* **2008**, *112*, 11054–11059.

(57) Butka, A.; Vale, V. R.; Saracsan, D.; Rybarsch, C.; Weiss, V. C.; Schröer, W. The Liquid- liquid Phase transition in Solutions of Ionic liquids with Halide Anions: Criticality and Corresponding States. *Pure Appl. Chem.* **2008**, *80*, 1613–1630.

(58) Lachwa, J.; Szydlowski, J.; Najdanovic-Visak, V.; Rebelo, L. P. N.; Seddon, K. R.; da Ponte, M. N.; Esperanca, J. M. S. S.; Guedes, H. J. R. Evidence for Lower Critical Solution Behavior in Ionic Liquid Solutions. *J. Am. Chem. Soc.* **2005**, *127*, 6542–6543.
(59) Ferreira, R.; Blesic, M.; Trindade, J.; Marrucho, I.; Canongia-Lopes, J. N.; Rebelo, L. P. N. Solubility of fluorinated compounds in a range of ionic liquids. Cloud-point temperature dependence on composition and pressure. *Green Chem.* **2008**, *10*, 918–928.
(60) Schröer, W.; Vale, V. R. Liquid-liquid phase separation in solutions of ionic liquids: phase diagrams, corresponding state analysis and comparison with simulations of the primitive model. *J. Phys. Condens. Matter* **2009**, *21*, 424119.
(61) Shiflett, M. B.; Niehaus, A. M. S. Liquid-Liquid Equilibria in Binary Mixtures Containing Substituted Benzenes with Ionic Liquid 1-Ethyl-3-methylimidazolium Bis(trifluoromethylsulfonyl)imide. *J. Chem. Eng. Data* **2010**, *55*, 346–353.
(62) Lachwa, J.; Szydlowski, J.; Makowska, A.; Seddon, K. R.; Esperanca, J. M. S. S.; Guedes, H. J. R.; Rebelo, L. P. N. Changing from an unusual high-temperature demixing to a UCST-type in mixtures of 1-alkyl-3-methylimidazolium bis{(trifluoromethyl)sulfonyl}amide and arenes. *Green Chem.* **2006**, *8*, 262–267.
(63) Heintz, A.; Lehmann, J.; Wertz, C.; Jacquemin, J. Thermodynamic properties of mixtures containing ionic liquids. 4. LLE of binary mixtures of [C2MIM][NTf2] with propan-1-ol, butan-1-ol, and pentan-1-ol and [C4MIM][NTf2] with cyclohexanol and 1,2-hexanediol including studies of the influence of small amounts of water. *J. Chem. Eng. Data* **2005**, *50*, 956–960.
(64) Wertz, Ch.; Tschersich, A.; Lehmann, J. K.; Heintz, A. Liquid-liquid equilibria and liquid-liquid interfacial tension measurements of mixtures containing ionic liquids. *J. Mol. Liq.* **2007**, *131*−*132*, 2–6.
(65) Heintz, A.; Lehmann, J.; Wertz, C. Thermodynamic properties of mixtures containing ionic liquids. 3. Liquid-liquid equilibria of binary mixtures of 1-ethyl-3-methylimidazolium bis(trifluoromethylsulfonyl)imide with propan-1-ol, butan-1-ol, and pentan-1-ol. *J. Chem. Eng. Data* **2003**, *48*, 472–474.
(66) Lachwa, J.; Morgado, P.; Esperanca, J. M. S. S.; Guedes, H. J. R.; Canongia Lopes, J. N.; Rebelo, L. P. N. Fluid-Phase Behavior of {1-Hexyl-3-methylimidazolium Bis(trifluoromethylsulfonyl) Imide, [C6mim][NTf2], + C2-C8 *n*-Alcohol Mixtures: Liquid-Liquid Equilibrium and Excess Volumes. *J. Chem. Eng. Data* **2006**, *51*, 2215–2221.
(67) Vale, V. R.; Rathke, B.; Will, S.; Schröer, W. Liquid-Liquid Phase Behavior of Solutions of 1-Octyl- and 1-Decyl-3-methylimidazolium Bis(trifluoromethylsulfonyl)imide ($C_{8,10}$mimNTf_2) in n-Alkyl Alcohols. *J. Chem. Eng. Data* **2010**, *55*, 2030–2038.
(68) Wohlfarth, C. *Static dielectric constants of pure liquids and binary liquid mixtures*; Landolt Börnstein, Numerical data and functional relationships in science and technology: New series IV/6; Springer: Berlin, 1991.
(69) Swatloski, R. P.; Holbrey, J. D.; Rogers, R. D. Ionic liquids are not always green: hydrolysis of 1-butyl-3-methylimidazolium hexafluorophosphate. *Green Chem.* **2003**, *5*, 361–363.
(70) Costa Gomes, M. F.; Canongia Lope, J. N.; Padua, A. A. H. Thermodynamics and Heterogeneity of Ionic Liquids. *Top. Curr. Chem.* **2009**, *290*, 161–183.
(71) Triolo, A.; Russina, O.; Bleif, H.; Cola, E. D. Nanoscale Segregation in room temperature ionic liquids. *J. Phys. Chem. B* **2007**, *111*, 4641–4644.
(72) Bradley, A. E.; Hardacre, C.; Holbrey, J. D.; Johnston, S.; McMath, S. E. J.; Nieuwenhuyzen, M. Small-Angle X-ray Scattering Studies of Liquid Crystalline 1-Alkyl-3-methylimidazolium Salts. *Chem. Mater.* **2002**, *14*, 629–635.
(73) Holbrey, J. D.; Reichert, W. M.; Rogers, R. D. Crystal structures of imidazolium bis(trifluoromethansulfonyl)imideionic liquid salts: the first organic salt with a cis-TFSI anion conformation. *Dalton Trans.* **2004**, 2267–2271.
(74) Lide, D. R. *Handbook of Chemistry and Physics*, 76th ed.; CRC Press: Boca Raton, 1995.
(75) Gutkowski, K.; Anisimov, M. A.; Sengers, J. V. Crossover criticality in ionic solutions. *J. Chem. Phys.* **2001**, *114*, 3133–3148.
(76) Guggenheim, E. A. The Principle of Corresponding States. *J. Chem. Phys.* **1945**, *13*, 253–261.

Received for review April 13, 2010. Accepted June 25, 2010. This work was supported by the German Research Foundation (DFG) within the priority program SPP-1191 “Ionic Liquids” (grants RA 1054/2-1 and SCHR 188/10-1).

JE100359X